

Comparison of Two Photolytic Calibration Methods for Nitrous Acid

Andrew J. Lindsay and Ezra C. Wood

Department of Chemistry, Drexel University, Philadelphia, PA, USA

Correspondence to: Ezra C. Wood (ew456@drexel.edu)

5 **Abstract.** Nitrous acid (HONO) plays an important role in tropospheric oxidation chemistry as it is a precursor to the hydroxyl radical (OH). Measurements of HONO have been ~~difficult historically~~ due to instrument interferences and difficulties in sampling and calibration. The traditional calibration method involves generation of HONO by reacting hydrogen chloride vapor with sodium nitrite followed by quantification by various methods (e.g., conversion of HONO to nitric oxide (NO) followed by chemiluminescence detection). Alternatively, HONO can be generated photolytically in the gas-phase by reacting NO with OH radicals generated by H_2O photolysis. In this work, we describe and compare two photolytic HONO calibration methods that were used to calibrate an iodide adduct chemical ionization mass spectrometer (CIMS). Both methods are based on the water vapor photolysis method commonly used for OH and HO_2 (known collectively as HOx) calibrations. The first method is an adaptation of the common chemical actinometry HOx calibration method, in which HONO is calculated based on quantified values for $[\text{O}_3]$, $[\text{H}_2\text{O}]$, $[\text{O}_2]$, and the absorption cross sections for H_2O and O_2 at 184.9 nm. In the second, novel method, HONO ~~is prepared in mostly N_2 ($[\text{O}_2] = 0.040\%$) and is simply quantified by measuring the NO_2 formed by the reaction of NO with HO_2 generated by H_2O photolysis. Both calibration methods were used to prepare a wide range HONO mixing ratios between of ~400 and 8,000 pptv. The uncertainty of the chemical actinometric calibration is 27 % (2 σ) and independent of HONO concentration. The uncertainty of the NO_2 proxy calibration is concentration-dependent, limited by the uncertainty of the NO_2 measurements. The NO_2 proxy calibration uncertainties (2 σ) presented here range from 4.5 to 24.4 % (at $[\text{HONO}] = 8,000$ pptv and $[\text{HONO}] = 630$ pptv, respectively) with a 10 % uncertainty associated with a mixing ratio of ~1,600 pptv, typical of values observed in urban areas at night. We also describe the potential application of the NO_2 proxy method to calibrating HOx instruments (e.g., LIF, CIMS) at uncertainties below 15 % (2 σ).~~

10

15

20

Deleted: historically

Deleted: the

Deleted: concentration

Deleted: determined based on the

Deleted: simultaneous measurements of

Deleted: from the

1 Introduction

Nitrous acid (HONO) is a source of the most important atmospheric oxidant – the hydroxyl radical (OH) – and can therefore play an important role in tropospheric oxidation chemistry. The hydroxyl radical ~~initiates~~ the removal of most trace gases from the atmosphere ~~leading to~~ the formation of secondary pollutants such as ozone (O_3) and secondary ~~aerosols~~ ~~organic~~ Photolysis of HONO yields OH and nitric oxide (NO):



Deleted: causes

Deleted: while initiating

Deleted: organic

Deleted: (SOA)

This reaction is the primary sink of HONO during the daytime leading to a typical chemical lifetime at mid-day of between 10-20 minutes at mid-latitudes. Sources of HONO include homogeneous formation (R2), direct emissions from combustion (vehicles, biomass burning, etc.) and soils, and numerous heterogeneous processes including heterogeneous reaction of NO_2 with moist terrestrial surfaces, photolysis of particulate nitrate (Ye et al., 2016; Ye et al., 2017), and photolysis of nitric acid (Ye et al., 2016).



45 The relative importance of these sources varies with environment (Jiang et al., 2022).

HONO photolysis has been reported as a major source of HOx (HOx = OH + HO₂) throughout the day in a variety of environments, including urban and highly polluted areas (Whalley et al., 2018; Slater et al., 2020; Ren et al., 2013; Lu et al., 2019) as well as more pristine environments (Villena et al., 2011; Jiang et al., 2020; Bloss et al., 2007). Vertical distributions of HONO, however, indicate that its significance as a HOx precursor may be limited to near ground level (Li et al., 2014; Young et al., 2012; Villena et al., 2011; Wong et al., 2012; Tuite et al., 2021; Jaeglé et al., 2018). HONO can also serve as an important source of HOx in indoor environments since sufficient UV light can penetrate windows and substantial HONO concentrations can result from various activities (e.g., cooking) (Gomez Alvarez et al., 2013; Wang et al., 2020).

HONO is notoriously difficult to measure. It can be formed via heterogeneous chemistry within sampling lines or an instrument's inlet. The resulting interferences may pose additional challenges in applying an instrument's zero or in calibration processes that alter the interfering species. Some intercomparison studies have shown substantial differences between HONO measurement techniques. A comparison of several HONO measurements in Beijing showed an overall mixed agreement with a few instruments disagreeing by more than a factor of two (Crilley et al., 2019). Measurements in Houston, Texas showed overall good agreement (within 20 %) between most instruments with larger differences of over 100 % observed for one of the instruments for some time periods (Pinto et al., 2014). Bourgeois et al. (in review, 2022) recently reported an 80 % difference between HONO measurements made by cavity-enhanced spectroscopy and iodide-adduct chemical ionization mass spectrometry (CIMS). Closer agreement for two instrument HONO comparisons has been reported by Stutz et al. (2010) (comparing differential optical absorption spectroscopy (DOAS) and mist-chamber ion chromatography (IC)), Cheng et al. (2013) (comparing Long-path absorption photometry (LOPAP) and stripping coil IC), and Dixneuf et al. (2022) (comparing LOPAP and cavity-enhanced absorption spectroscopy), though many of these studies report considerable deviations when HONO mixing ratios were less than ~100 pptv.

60 Calibrations for HONO are challenging as this compound is not commercially available and rather must be prepared in situ. Most commonly, HONO is prepared by reacting hydrogen chloride vapor with sodium nitrite (Febo et al., 1995):



65 This method presents several challenges. A stable source of HCl is required, usually from a heated aqueous solution, a gas cylinder, or a permeation tube. Consistent mixing between the HCl and the NaNO₂ powder is required. These calibrations also require substantial warmup times (often hours) to ensure source stability, though some recent versions report faster warmup periods (e.g., < 10 min reported by Villena and Kleffmann (2022)). High HONO concentrations (above 1 ppmv) are often produced, requiring dilution, though the temporary unrealistic HONO concentrations can lead to significant HONO loss by its self-reaction and inaccurate HONO quantification. A recent, noteworthy version of this calibration improves upon this concentration issue and has the ability to produce [HONO] on the order of tens of pptv (Lao et al., 2020). The generated HONO can be quantified by various methods including theoretical calculation (Villena and Kleffmann, 2022), conversion to NO followed by chemiluminescence detection (Lee et al., 2012; Lao et al., 2020; Villena and Kleffmann, 2022), thermal conversion to NO₂ followed by NO₂ quantification (Gingersty and Osthoff, 2020), and conversion to aqueous nitrite followed by derivatization and detection by UV-vis (Peng et al., 2020). The calibration uncertainty depends on the output stability of the HONO source and the quantification technique used. Villena and Kleffmann (2022) demonstrate using two separate techniques that overall calibration uncertainties can be well below 10 % (2 σ).

Deleted: For a Beijing, China based study, a

Deleted: major differences observed for a few techniques

Deleted: several instruments to mostly agree in capturing variations in HONO, though there were differences in the magnitude of presented [HONO] value

Deleted: s

Deleted: it

Deleted: This method typically produces

Deleted: h

90 More recently, photolytic HONO sources have been utilized. Humidified air is exposed to ultraviolet (UV) light to photolyze H₂O to produce an equal mixture of OH and HO₂, which in the presence of excess NO then converts to HONO. This HONO output is stable within seconds (i.e., the initial UV lamp warm up time) and is tunable by altering humidity, UV flux, or UV exposure time. The HONO formed has been quantified based on the water vapor mixing ratio, water vapor absorption cross section, the UV flux, and the UV exposure time. This quantification approach thus far has been used to calibrate HONO photo-fragmentation instruments that detect OH using laser-induced fluorescence spectroscopy (Dyson et al., 2021; Bottorff et al., 2021). The HONO formed from a photolytic source has also been quantified by thermal dissociation followed by measurement of the NO₂ produced (Veres et al., 2015). These methods have an uncertainty of 30 to 36% (2 σ), similar to the uncertainty for HO_x calibrations based on water vapor photolysis (Dusander et al., 2008). In this manuscript, we present an alternative photolytic HONO calibration that we refer to as the “NO₂ proxy” method. This method requires a direct NO₂ measurement that is used as a ‘proxy’ to quantify HONO concentrations. We compare this new proxy calibration to the more standard photolytic calibration method as performed by Bottorff et al. (2021) and Dyson et al. (2021). This method has a lower uncertainty (typically ~10%, 2 σ) and unlike the actinometric method does not require characterization of the mercury lamp emission spectrum.

2 Methods

2.1 Instrumentation

105 A Cavity Attenuated Phase Shift (CAPS) spectrometer ([Aerodyne Research, Inc.](#)) was used to detect NO₂ (Kebabian et al., 2008). The CAPS also indirectly measured O₃ as it was converted to NO₂ by reaction with excess NO. The CAPS instrument was calibrated using a 2B Technologies Model 306 O₃ Calibration Source. Ozone outputs were varied between 10 and 300 ppbv with greater than 99.99 % conversion efficiency to NO₂ by reaction with excess NO ([NO] = 1.82 ppmv) within approximately 15 m of FEP tubing (i.d. = 0.476 cm; residence time = 17.1 s, pseudo-first order rate constant of 0.8 s⁻¹). The manufacturer stated accuracy of this O₃ calibrator is 2 % (2 σ), though no recent factory calibrations have been conducted. Therefore, a second calibration was conducted with a Thermo Environmental Instruments 49C O₃ Calibrator, which agreed to within 2.5 %. We assign an uncertainty of 4 % (2 σ) to the NO₂ measurements to account for possible drift in accuracy. Temperature and relative humidity (RH) measurements were made using two Vaisala HMP60 probes and used, along with pressure measurements, to calculate H₂O(_g) mixing ratios. Both probes agreed with a new RH/T replacement sensor (manufacturer stated uncertainty: 3 %) to within 3 %. We assign an uncertainty of 5 % (2 σ) to our determined H₂O mixing ratios.

110 A High-Resolution Chemical Ionization Time of Flight Mass Spectrometer (HR-ToF-CIMS, Tofwerks/Aerodyne Research, Inc.) was used to detect HONO (Bertram et al., 2011; Lee et al., 2014). HONO and concomitant gases are ionized within a laboratory-built ion-molecule reactor (IMR) using reagent iodide (I⁻) ions. Our lab-built IMR is internally coated with PTFE and sampled the calibration gas at a flow rate of 2.10 SLPM through a stainless-steel critical orifice (nominal diameter of 0.48 mm). Iodide (I⁻) reagent ions in N₂ ([Airgas, industrial grade](#)) were sampled at 2.20 SLPM through a similar critical orifice perpendicular to the main sample flow. The I⁻ was prepared by exposing dilute methyl iodide (CH₃I) from a permeation tube ([VICI Metronics](#)) to a ²¹⁰Po radioactive source. Humidified N₂ was also added to the IMR perpendicular to the main sample flow at a flow rate of 0.365 SLPM. The pressure in the IMR was held at 80 mbar, controlled by adjusting a valve to a scroll pump (Agilent Technologies IDP-7).

125 Ions are separated by mass-to-charge ratio (m/z) at a mass resolving power of near 5000 m/Δm. We monitor the HONO iodide adduct I(HONO)⁻ at 173.90575 m/z. The peak-fitting software (TofWare) accounts for the overlapping contribution from the ¹³C

Deleted: by inferring the UV flux by measuring the O₃ produced from O₂ photolysis

Deleted: and by

Deleted: of the HONO

Deleted: agreed to within 2.5% with a

Deleted: .

Deleted: 3

Deleted: The

Deleted: the

formic acid $I(^{13}\text{CH}_2\text{O}_2)^+$ peak at 173.91342 m/z. We account for the humidity dependence of the instrumental response by determining the mole fraction of $\text{H}_2\text{O}_{(\text{g})}$ ($\chi_{\text{H}_2\text{O}}$) in the IMR by measuring the RH and temperature of the IMR in the exhaust of the scroll pump. [See the supplement for more information regarding humidity effects for the HONO ionization chemistry \(see Sect. S1.2\).](#) Analytical parameters including the limit of detection, precision, and linear range of these HONO measurements are also [detailed within the supplement \(see Sect. S1.1\).](#)

2.2 Calibration Methods

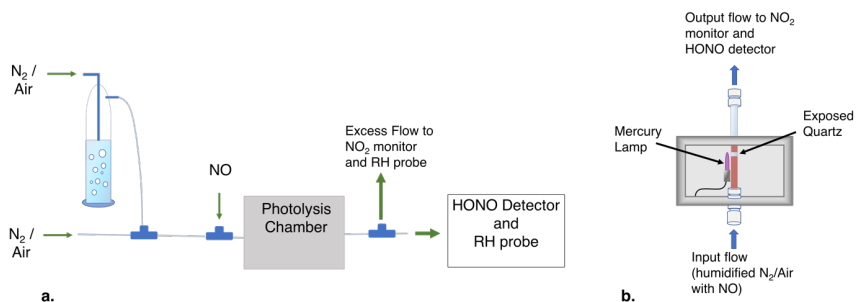


Figure 1: Schematic of the experimental setup (a.) and the photolysis chamber (b.). Not shown: small flow of air when using N_2 as the carrier gas (a.), and the purge flow of N_2 (b.).

We calibrate HONO using two variations of the water vapor HO_x calibration method: one is a modification of the standard actinometric HO_x photolytic calibration and the other we refer to as the “ NO_2 proxy” calibration. These calibration methods mainly differ in how HONO is quantified. In both methods, HONO was produced nearly identically. [Air \(Airgas, Ultra Zero grade; \$\[\text{O}_2\] = 21 \pm 1 \%\$ \)](#) for the actinometric method or N_2 ([Airgas, industrial grade](#)) for the NO_2 proxy calibration is [humidified with HPLC \(high-performance liquid chromatography\) grade water \(Fisher Chemical\)](#), mixed with NO ([Airgas, \$41.02 \pm 2.05 \text{ ppmv in N}_2\$](#)), and then exposed to 184.9 nm ultraviolet radiation from a low-pressure mercury lamp (Jelight 78-2046-1). [While in the experiments presented in this manuscript we used industrial grade \$\text{N}_2\$ for the humidified CIMS IMR inflow \(mentioned in Sect. 2.1\) and as the \$\text{NO}_2\$ proxy calibration carrier gas, we have used ultra-high purity \$\text{N}_2\$ \(Airgas\) in previous experiments. We find no differences between the calibration results acquired using different grades of \$\text{N}_2\$.](#) The resulting OH and HO₂ from water photolysis form HONO by reaction with excess NO (R4-6a and R2).



The HO₂ to HONO pathway is limited by the [small fraction of R5 that forms \$\text{HNO}_3\$ rather than OH and \$\text{NO}_2\$](#) :



A schematic of the setup used for both calibrations is shown in [Fig. 1](#). The mercury lamp is housed within a 10.8 cm \times 26.7 cm \times 10.2 cm photolysis chamber (Fig. 1b), and the volume surrounding the lamp is purged with dry N_2 (purge not shown). The

Deleted: following reaction

Deleted: Figure

165 humidified air-NO mixture is transported past the mercury lamp within a partially exposed quartz tube (I.D. = 1.04 cm, total length
= 26.7 cm; exposed length = ~ 0.5 cm). HONO sample concentrations are controlled by adjusting the lamp flux with a Variac
Variable transformer, adjusting the relative flow rates of the dry and humidified zero air/N₂, or adjusting the absolute flow rates to
alter the lamp exposure time. For our example calibrations discussed in this manuscript, we typically used a main N₂ or air flow
rate of 5 SLPM with an addition of 200 sccm of 41.02 ppmv NO in N₂ for a total flow rate of 5.20 SLPM and a diluted NO mixing
ratio of 1.58 ppmv. Pseudo-first order rate constants calculated using this [NO] for R6a and R2 are 322 s⁻¹ and 295 s⁻¹, respectively.
70 Under these conditions, HO_x is converted to HONO within 0.02 s inside the remaining 11.4 cm of the quartz tube. The [NO]
chosen must be high enough to minimize OH and HO₂ wall losses. We have ensured that this NO mixing ratio is sufficient in
separate experiments by confirming that no additional HONO signal results at increased [NO] values. Possible HONO formation
75 by additional photolytic processes (specifically involving the surfaces of the quartz photolysis tube) was tested by monitoring
CIMS I(HONO) signals during additional experiments. These experiments include exposing dry carrier gas ([NO] = 1.58 ppmv)
to 184.9 nm radiation (i.e., exposure to UV without H₂O photolysis), exposing humidified carrier gas ([NO] = 0 ppmv) to 184.9
nm radiation (i.e., to investigate if HONO is formed by heterogenous reactions involving H₂O or HO_x with NO, NO₂, or HNO₃
adsorbed on the quartz tube), and exposing humidified carrier gas ([NO] = 1.58 ppmv) to the 254 nm radiation from a separate
80 mercury lamp (Jelight 81-3306-2) in which the 184.9 nm emission is blocked (i.e., the carrier gas matches calibration conditions
and is exposed to UV radiation but without H₂O photolysis). These tests indicate no appreciable HONO formation by other
photolytic processes.▼

Deleted: 26.7 cm

Deleted: ZA

Deleted: (Airgas)

Deleted: (the reactions that form HONO)

Deleted: The resulting calibration gas was sampled by the CIMS (2.1 SLPM) and the NO₂ monitor (1.1 SLPM). The excess flow was vented past an RH/T probe to determine the water mixing ratio in the photolysis cell. A second RH/T probe quantified the water mixing ratio in the CIMS IMR as previously mentioned in Sect. 2.1. Details of the two calibration methods are described in the following sections.

185 The resulting calibration gas enters a PFA tee and is arranged so that the air travels straight to the CIMS (2.1 SLPM) while
the remaining flow (~ 3.1 SLPM) makes a 90° turn for the CAPS line which includes a vent. The gas flow is initially laminar within
the quartz photolysis tube (Reynolds number ≈ 600). This results in an initial [HO₂] (and therefore [HONO]) radial gradient in
which the greatest concentrations exist near the flow tube walls (i.e., where the flow rates are lower and the UV exposure times
longer). Turbulence is induced by the sudden changes in tube inner diameter at the quartz tube exit (reducing union) and upon
entering the PFA tee. The air is therefore most likely well mixed prior to being split within the PFA tee. The excess flow within
the CAPS line (~ 2 SLPM) was vented past an RH/T probe to determine the water mixing ratio in the photolysis cell. A second
190 RH/T probe quantified the water mixing ratio in the CIMS IMR as previously mentioned in Sect. 2.1. Details of the two calibration
methods are described in the following sections.

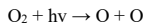
2.2.1 Actinometric Calibration

The water vapor photolysis calibration method has been used for several decades to calibrate OH and HO₂ measurements
(Stevens et al., 1994; Lanzendorf et al., 1997; Dusanter et al., 2008). The concentration of HO_x, and therefore HONO, is calculated
from the time-integrated photolysis of water vapor:

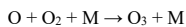
$$195 [HONO] \approx [HO_x] = (F \cdot t)[H_2O]\sigma_{H_2O}\phi_{HO_x} \quad (1)$$

where F is the photon flux at 184.9 nm, t is the UV irradiation time, σ_{H_2O} is the absorption cross section of water at 184.9 nm, and
 ϕ_{HO_x} is the quantum yield of HO_x from water photolysis and equal to 2. F can be quantified using direct actinometric measurements
(e.g., using a calibrated phototube), and t can be quantified via characterization of the flow rates and photolysis cell geometry
(Faloona et al., 2004). Alternatively, and more commonly among HO_x measurement groups, the product $F \cdot t$ can be determined via
200 “chemical actinometry” (Schultz et al., 1995). In the O₂-O₃ chemical actinometry method, the concentration of O₃ produced by
photodissociation of O₂ at 184.9 nm is used to determine $F \cdot t$.

Deleted: W



(R7)



(R8)

215

The product of the lamp flux and the exposure time, i.e., the $(F \cdot t)$ term, is given by Eq. (2), in which σ_{O_2} is the absorption cross section of O_2 at 184.9 nm and Φ_{O_3} is quantum yield of O_3 from O_2 photolysis ($\Phi_{\text{O}_3} = 2$):

Deleted: 2

$$(F \cdot t) = \frac{[\text{O}_3]}{[\text{O}_2]\sigma_{\text{O}_2}\Phi_{\text{O}_3}} \quad (2)$$

Substituting this expression for $F \cdot t$ into Eq. (1) gives Eq. (3):

220

$$[\text{HONO}] \approx [\text{HOx}] = \frac{[\text{O}_3]}{[\text{O}_2]\sigma_{\text{O}_2}} [\text{H}_2\text{O}]\sigma_{\text{H}_2\text{O}} \quad (3)$$

225

The effective value for σ_{O_2} must be experimentally determined for the individual mercury lamp at the experimental O_2 optical depth. This is required because the emission profile near 14.9 nm, which comprises two peaks due to self-reversal, can vary from lamp to lamp and with operating conditions, and the O_2 absorption spectrum steeply decreases near the mercury lamp emission maximum (Lanzendorf et al., 1997). We use an experimentally determined σ_{O_2} value of $1.4 \times 10^{-20} \text{ cm}^2 \text{ molec}^{-1}$ for the mercury lamp used for these experiments. The JPL-recommended value of $7.1 \times 10^{-20} \text{ cm}^2 \text{ molec}^{-1}$ was used for $\sigma_{\text{H}_2\text{O}}$ (Burkholder et al., 2020). The value of $[\text{O}_2]$ is based on the flows mentioned in Sect. 2.2 and is equal to $20.1 \pm 1.0 \text{ %}$. The O_2 optical depth is 0.033, and the O_2 column density (within the photolysis tube center) is $2.4 \times 10^{18} \text{ molecules cm}^{-2}$. For typical operating conditions, the value of $F \cdot t$ and an estimated photon flux F (calculated using an approximate gas exposure time) are $3.48 \times 10^{12} \text{ photons cm}^{-2}$ and $7.1 \times 10^{14} \text{ photons cm}^{-2} \text{ s}^{-1}$, respectively. The value of $[\text{O}_3]$ here was near 20 ppbv and determined with the CAPS NO_2 monitor after its reaction with NO , forming NO_2 . This is measured with dry air flowing in the photolysis chamber so that the NO_2 measured is solely from the reaction of NO with O_3 and not HO_2 . These $F \cdot t$ and $[\text{O}_3]$ values are high compared to those used for most O_3 actinometry HOx calibrations, in which $[\text{O}_3]$ is often less than 1 ppbv (e.g., Faloona et al. (2004)), but are comparable to those used by Dusander et al. (2008). High $F \cdot t$ values were used so that typical ambient HONO concentrations (ranging up to several ppbv) could be prepared. $[\text{H}_2\text{O}]$ is determined using the measured RH, temperature, and pressure. The uncertainties of the variables in Eq. (3) are discussed in Sect. S3 of the supplement. The combined uncertainty (2σ) for $[\text{HOx}]$ (and therefore $[\text{HONO}]$) calculated using this equation is 27 % (see supplement for details).

230

We apply a small correction to the value for $[\text{HOx}]$ calculated in Eq. (3) in order to obtain $[\text{HONO}]$. This correction accounts for the incomplete conversion of HO_2 to HONO due to R6b.

235

$$[\text{HONO}] = (0.5 + 0.5 \cdot \frac{1}{1+\beta}) \cdot [\text{HOx}] \quad (4)$$

240

Equation 4 includes the variable β , which is the relative rate or product ratio of R6b to R6a (i.e., $\beta = k_{\text{R6b}}/k_{\text{R6a}} = [\text{HNO}_3]/[\text{NO}_2]$) and depends on temperature, pressure, and humidity (Butkovskaya et al., 2007; Butkovskaya et al., 2009). The term $1/(1+\beta)$ in Eq. (4) represents a traditional branching ratio (i.e., $k_{\text{R6b}}/(k_{\text{R6a}}+k_{\text{R6b}}) = [\text{HNO}_3]/([\text{NO}_2]+[\text{HNO}_3])$). For the experiments conducted, the value of β is at most 0.04, leading to a 2 % correction to equation 1. See Sect. S2 of the supplement for information regarding the formulation of Eq. (4) and the calculation of β .

245

The CIMS response to HONO is determined by acquiring a background by briefly toggling off the mercury lamp. This background CIMS signal is humidity dependent, so a background is taken at each humidity setting. Background CIMS $\text{I}(\text{HONO})$ signals are elevated during calibrations due to impurities in the NO flow.

Deleted: to account for the non-ideal overlap between the lamp emission spectrum and the O_2 absorption spectrum
 Deleted: a
 Deleted: x
 Deleted: for σ_{O_2}
 Deleted: We use the
 Deleted: x
 Moved (insertion) [1]
 Deleted: The O_3 concentration within Eq. (3) is
 Deleted: $[\text{H}_2\text{O}]$ is determined using the measured RH, temperature, and pressure.

Deleted: fraction that includes β
 Deleted: Values
 Deleted: are
 Deleted: 1
 Moved up [1]: The O_3 concentration within Eq. (3) is determined with the CAPS NO_2 monitor after its reaction with NO , forming NO_2 . This is measured with dry air flowing in the photolysis chamber so that the NO_2 measured is solely from the reaction of NO with O_3 and not HO_2 . $[\text{H}_2\text{O}]$ is determined using the measured RH, temperature, and pressure.
 Deleted: The
 Deleted: contributes to the CIMS background HONO signal but is constant over time.

2.2.2 Proxy Calibration

For the NO₂ proxy calibration method, we determine [HONO] from the measured value of [NO₂] formed from R6a during 275 HONO production. For each H₂O molecule photolyzed (R4), nearly one NO₂ and two HONO molecules are produced. Therefore, [HONO] is simply given by the measured [NO₂] (Eq. (5)):

$$[\text{HONO}] = (2 + \beta) \cdot [\text{NO}_2] \quad (5)$$

where β is added to account for the minor HNO₃ product of the HO₂ + NO reaction (R6b).

Deleted: w

For the proxy calibration we use humidified N₂ rather than air and include a small addition of 10 sccm of zero air prior to lamp 280 exposure (not shown in the Fig. 1 schematic). The resulting low O₂ concentration ($[\text{O}_2] = 0.040 \pm 0.002 \%$) is sufficient for the full conversion of H to HO₂ (R5) but results in a negligible amount of O₃ formed by O₂ photolysis (R7-R8), confirmed by toggling the UV source on and off with dry carrier gas flowing. The pseudo-first order rate constant for the H to HO₂ conversion (R5) is $1.1 \times 10^4 \text{ s}^{-1}$ for this [O₂] value. HONO concentrations are quantified using background subtracted [NO₂] values in Eq. (5), which are 285 typically acquired by toggling the mercury lamp off and on. The CIMS signal response is determined simultaneously. A “direct” NO₂ detection method is highly recommended over indirect methods that rely on NO detection as the high NO mixing ratios would result in degraded precision. For this study we used a CAPS instrument but other methods like cavity ring down spectroscopy (CRDS), laser-induced fluorescence (LIF), or oxygen anion CIMS (e.g., Novak et al. (2020)) would be acceptable.

Deleted: N₂

3 Results and Discussion

Time series data for the proxy calibration method are shown in Fig. 2. The CAPS NO₂ measurement and the CIMS HONO signal normalized to one million counts per second of reagent ion (‘ncps’) are shown at a constant humidity (RH = 29 %, $\chi_{\text{H}_2\text{O}} = 0.0065$, T = 19.3 °C, P = 760 Torr within the photolysis cell and RH = 19 %, $\chi_{\text{H}_2\text{O}} = 0.0042$, T = 19.2 °C, P = 760 Torr within the 295 CIMS IMR exhaust). During the first 120 s shown in Fig. 2, HONO is formed by H₂O photolysis via the mercury lamp 184.9 nm emission. This leads to the stable I(HONO) signal in the CIMS along with enhanced [NO₂] produced by R6a and measured by the CAPS monitor. Background I(HONO) and NO₂ signals are determined by toggling off the mercury lamp (shown at 121 s). The CIMS sensitivity (ncps ppt⁻¹) is equal to the quotient of the normalized background subtracted CIMS signal and the quantified [HONO] which is calculated by Eq. (5).

Deleted: is

Deleted: per

Deleted: per second

Deleted: RH setting

Deleted: 40

Deleted:) (

Deleted: X $\times 10^{-3}$) within the H₂O photolysis

Deleted: cell

Deleted: 95

Deleted: 96

A multipoint NO₂ proxy calibration curve (Fig. 3) shows the linear CIMS signal response to [HONO]. This calibration was conducted at a constant relative humidity (RH = 28 %, $\chi_{\text{H}_2\text{O}} = 6.22 \times 10^{-3}$, T = 19.3 °C, P = 760 Torr) within the photolysis cell and 300 RH = 18 %, $\chi_{\text{H}_2\text{O}} = 3.88 \times 10^{-3}$, T = 19.2 °C, P = 760 Torr) within the CIMS IMR exhaust, and [HONO] was adjusted by altering the mercury lamp flux with a Variac variable transformer. The slope of this curve, $2.89 \pm 0.34 \text{ ncps ppt}^{-1}$ (2σ), is the CIMS sensitivity to HONO for this particular water mole fraction within the CIMS IMR ($\chi_{\text{H}_2\text{O}} = 3.88 \times 10^{-3}$). HONO mixing ratios ranged from approximately 400 pptv to 3500 pptv, thus demonstrating that a wide range in HONO concentrations can easily be prepared. The uncertainty for the quantified [HONO] values from Eq. (5) (i.e., the x-error bars) are obtained by adding in quadrature three 305 terms: 1.) the relative uncertainty of the NO₂ background subtraction (based on the 5 s average precision of 27 pptv), 2.) the NO₂ calibration uncertainty (3%, 2σ), and finally 3.) the relative uncertainty associated with the $(2 + \beta)$ expression (typically 0.14%, 2σ). The uncertainty in the normalized CIMS signal is obtained by adding in quadrature the 15 s precision of the I(HONO) signal with that of the reagent ion. The 2σ error bars range from 6.1 to 34.8 % for quantified [HONO] and 1.7 to 2.9 % in the CIMS HONO signal. The Fig. 3 slope (i.e., the CIMS sensitivity to HONO) and its uncertainty were determined using the York bivariate

Deleted: of water

Deleted: y

Deleted: is

Deleted: error

Deleted: 5.6

Deleted: 6.8

Deleted: 11

Deleted: .2

Deleted: as

330

linear regression method (York et al., 2004). The uncertainty calculations are discussed in greater detail in Sect. S4.1 of the supplement.

Deleted: 2

335

A comparison between the more standard O₃ actinometry based calibration and the new proxy calibration method is shown in Fig. 4. CIMS sensitivities as determined by single point calibrations are shown for a variety of $\chi_{\text{H}_2\text{O}}$ values. The two calibration methods were conducted consecutively and agree within their provided 2σ errors. Sensitivities ranged from 1.5 to 5.3 ncps ppt¹ with the greatest values observed at low $\chi_{\text{H}_2\text{O}}$ settings. The CIMS IMR $\chi_{\text{H}_2\text{O}}$ values ranged from 1.77×10^{-3} to 8.25×10^{-3} and corresponded to a photolysis cell RH range of 4.1 to 71 % and photolysis cell $\chi_{\text{H}_2\text{O}}$ values of 0.93×10^{-3} to 16×10^{-3} (average T = 19.6 °C; P = 760 Torr). The sensitivity determined by the Fig. 3 multipoint calibration (2.89 ± 0.34 ncps ppt¹ at CIMS IMR $\chi_{\text{H}_2\text{O}} = 3.88 \times 10^{-3}$) is consistent with those shown in Fig. 4 at similar $\chi_{\text{H}_2\text{O}}$ values. These CIMS sensitivities are also in line with literature values (Peng et al., 2020; Bourgeois et al., in review, 2022). Unique to this figure is the use of the CIMS IMR $\chi_{\text{H}_2\text{O}}$ to track humidity dependence rather than the partial pressure of H₂O (Lee et al., 2014), the specific humidity (Novak et al., 2020), or the CIMS signal ratio of the iodide water adduct I(H₂O)[·] (m/z 145) to reagent ion I[·] (m/z 127) (Lee et al., 2014; Peng et al., 2020; Veres et al., 2015; Veres et al., 2020). The use of $\chi_{\text{H}_2\text{O}}$ allows for a more direct comparison to other CIMS instruments that may use different IMR pressures and quadrupole voltage settings that govern the I(H₂O)[·] to I[·] ratio. See the supplement for more information regarding humidity effects on ionization chemistry (Sect. S1.2).

340

The uncertainty in the CIMS sensitivity for the single-point proxy calibration points in Fig. 4 is determined by combining in quadrature the relative uncertainty of the background subtracted CIMS signal with that of the quantified [HONO] value. The calculation for quantified [HONO] uncertainty and CIMS uncertainty is previously mentioned in the text regarding Fig. 3, though the CIMS uncertainty here slightly differs due to the background subtraction (see Sect. S4.2 the supplement). As mentioned previously, the total uncertainty depends on the quantified [HONO] value, which ranged from 630 (at the lowest $\chi_{\text{H}_2\text{O}}$ value) to 7,800 pptv (at the greatest $\chi_{\text{H}_2\text{O}}$ value) for the proxy calibration results shown in Fig. 4. The uncertainty for the greatest [HONO] values (corresponding to the highest $\chi_{\text{H}_2\text{O}}$ settings) are dominated by the 4 % 2σ uncertainty of the NO₂ measurement. At the lowest [HONO] values (shown at lowest $\chi_{\text{H}_2\text{O}}$ settings), larger uncertainties occur and are dominated by the precision in NO₂ measurements due to the background subtraction. Therefore, the uncertainty can be minimized by using higher HONO concentrations. The presented 2σ uncertainty in sensitivity using the proxy method ranged from 5.1 to 25.5 % with the [HONO] quantification alone accounting (from E.q. (4)) for 4.5 to 24.4 %. These proxy calibration uncertainties for [HONO] fall well below the 27 % 2σ uncertainty associated with the standard O₃ actinometry calibration. The 2σ uncertainty in sensitivities determined by our actinometry calibrations (i.e., the 27 % method uncertainty combined with precision of the CIMS measurement) varies from 27.1 to 28.8 %. The proxy calibration therefore allows for lower uncertainties compared to the standard actinometry calibration, especially at high [HONO] values.

Deleted: users

345

The uncertainty in the CIMS sensitivity for the single-point proxy calibration points in Fig. 4 is determined by combining in quadrature the relative uncertainty of the background subtracted CIMS signal with that of the quantified [HONO] value. The calculation for quantified [HONO] uncertainty and CIMS uncertainty is previously mentioned in the text regarding Fig. 3, though the CIMS uncertainty here slightly differs due to the background subtraction (see Sect. S4.2 the supplement). As mentioned previously, the total uncertainty depends on the quantified [HONO] value, which ranged from 630 (at the lowest $\chi_{\text{H}_2\text{O}}$ value) to 7,800 pptv (at the greatest $\chi_{\text{H}_2\text{O}}$ value) for the proxy calibration results shown in Fig. 4. The uncertainty for the greatest [HONO] values (corresponding to the highest $\chi_{\text{H}_2\text{O}}$ settings) are dominated by the 4 % 2σ uncertainty of the NO₂ measurement. At the lowest [HONO] values (shown at lowest $\chi_{\text{H}_2\text{O}}$ settings), larger uncertainties occur and are dominated by the precision in NO₂ measurements due to the background subtraction. Therefore, the uncertainty can be minimized by using higher HONO concentrations. The presented 2σ uncertainty in sensitivity using the proxy method ranged from 5.1 to 25.5 % with the [HONO] quantification alone accounting (from E.q. (4)) for 4.5 to 24.4 %. These proxy calibration uncertainties for [HONO] fall well below the 27 % 2σ uncertainty associated with the standard O₃ actinometry calibration. The 2σ uncertainty in sensitivities determined by our actinometry calibrations (i.e., the 27 % method uncertainty combined with precision of the CIMS measurement) varies from 27.1 to 28.8 %. The proxy calibration therefore allows for lower uncertainties compared to the standard actinometry calibration, especially at high [HONO] values.

Deleted: method

Deleted: error

Deleted: 2

Deleted: is dependent

Deleted: shown Fig. 4

Deleted: The uncertainty at the lowest $\chi_{\text{H}_2\text{O}}$ settings, which were also the lowest HONO concentrations, were dominated by [HONO] quantification

Deleted: stemming from the

Deleted: of NO₂

Deleted: 8.7

Deleted: 38

Deleted: 8

Deleted: All presented

Deleted: besides the two at lowest $\chi_{\text{H}_2\text{O}}$ values (i.e., the smallest [HONO] values)

Deleted: 30

Deleted: is

Deleted: a general improvement over

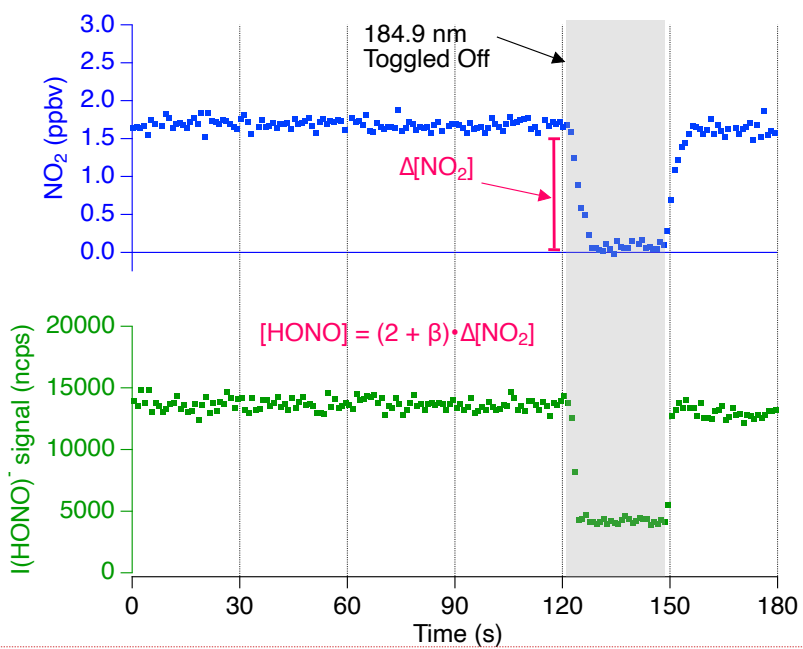
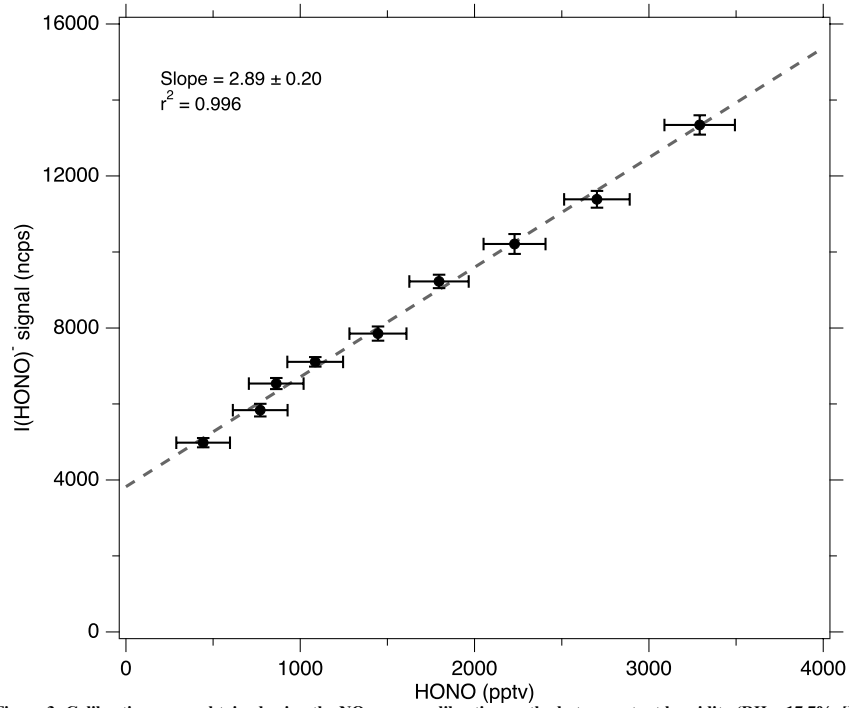


Figure 2: One-second averaged time series data for a proxy calibration at a constant relative humidity. The iodide HONO adduct signal (cps) is shown normalized per one million reagent ions (ncps). The shaded section represents the period in which the 184.9 nm mercury lamp is toggled off to obtain background $[NO_2]$ and HONO signal. The NO_2 concentration is shown with an offset so that background values are near 0 ppbv. The resulting difference in NO_2 indicates that approximately 3.000 pptv [HONO] is sampled by the CIMS.

Deleted: (Veres et al., 2015; Bottorff et al., 2021; Dyson et al., 2021)(Bottorff et al., 2021)¶

Deleted: highlighted



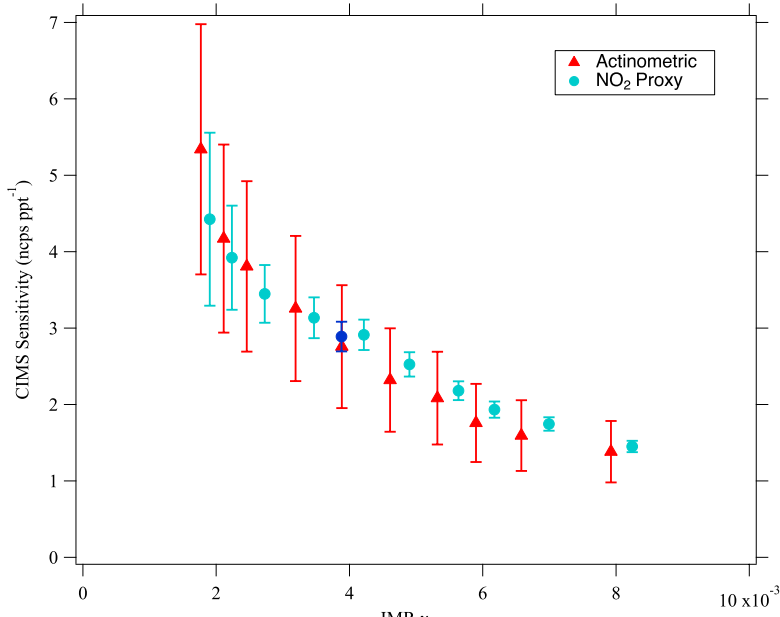


Figure 4: Comparison of the two HONO calibration methods for a range of $\chi_{\text{H}_2\text{O}}$ within the CIMS IMR. The sensitivity determined by the multipoint calibration (i.e., the Fig. 3 slope) is plotted as the dark blue circle. Error bars represent $\pm 2 \sigma$ uncertainties. [HONO] ranged from 470 pptv (at the lowest $\chi_{\text{H}_2\text{O}}$ value) to 7,710 pptv (at the greatest $\chi_{\text{H}_2\text{O}}$ value) for the actinometric calibration. [HONO] similarly ranged 630 pptv to 7,820 pptv for the NO₂ proxy calibration.

4 Application to HO_x Calibrations

In addition to its use described herein for HONO calibrations, the NO₂ proxy method can also be used to determine the prepared HO_x concentration (i.e., prior to its reaction with NO), which differs from [HONO] by only a few percent depending on the value of β .

$$[\text{HO}_x] = (2 + 2\beta) \cdot [\text{NO}_2] \quad (6)$$

Directly using this method to calibrate a HO_x instrument (e.g., LIF, HO_x-CIMS, or perCIMS) is likely not feasible as the described calibration is performed in N₂ rather than air (i.e., the composition of the calibration carrier gas should be identical to that for ambient air) and requires high NO mixing ratios that could complicate the operation of a HO_x instrument more than it does for our iodide CIMS.

The application of an NO₂ proxy calibration for a HO_x instrument would likely require two consecutive steps. First an NO₂ proxy calibration would be performed as described in this manuscript (with high [N₂], high [NO], and only the NO₂ instrument sampling). Second, the N₂ and NO flows would be replaced with zero air, and the resulting calibration mixture, which would have the same HO_x concentration as determined by the NO₂ proxy calibration, would then be sampled by a HO_x instrument. Additional concentrations of HO_x could be prepared by altering and tracking [H₂O]:

420
$$[\text{HOx}] = \frac{[\text{HOx}]_{\text{proxy}}}{[\text{H}_2\text{O}]_{\text{proxy}}} [\text{H}_2\text{O}] \quad (7)$$

where the ‘proxy’ designation refers to the corresponding values of $[\text{HOx}]$ (quantified via Eq. 6) and $[\text{H}_2\text{O}]$ during the proxy calibration step (i.e., high $[\text{NO}]$ and N_2 as the carrier gas). The quotient of $[\text{HOx}]$ and $[\text{H}_2\text{O}]$ is equal to the product of the constants $F \cdot t \cdot \sigma_{\text{H}_2\text{O}} \cdot \Phi_{\text{HOx}}$ that appear in Eq. 1.

425 The uncertainty in $[\text{HOx}]$ will likely range 5 to 15 % (2σ), similar to that for $[\text{HONO}]$ quantified via proxy calibration, mainly dependent on the $[\text{NO}_2]$ measurement uncertainty. While the accuracy in H_2O measurements should not contribute to the Eq. 7 $[\text{HOx}]$ uncertainty as it effectively cancels out, the precision in the $[\text{H}_2\text{O}]$ measurements would have to be accounted for. The uncertainty for this proposed method is exceptional compared to typical HOx calibrations in which total uncertainties are often above 25 % (2σ) based on the combination of Eq. (1) parameters of $F \cdot t$, $\sigma_{\text{H}_2\text{O}}$, and $[\text{H}_2\text{O}]$.

430 5 Conclusions

Deleted: ¶

435 Two photolytic HONO calibration methods based on reacting NO with the HOx generated by H_2O photolysis at 184.9 nm were presented. This includes a novel approach in which HONO is quantified using the NO_2 formed by the $\text{HO}_2 + \text{NO}$ reaction as a proxy. The proxy method compares well with the O_3 actinometry based calibration while also having the benefit of a simpler calculation that avoids the need to characterize the emission spectrum of the mercury lamp used. In addition, this proxy method has improved uncertainties, typically between 4.5 and 10 % (2σ) – lower than the 27% 2σ uncertainty associated with the actinometric calibration method. We also detail the potential application of a NO_2 proxy calibration for HOx calibrations, in which we anticipate exceptional 2σ uncertainties of below 15 %. These photolytic calibrations require a direct NO_2 measurement, a 184.9 nm light source, and a simple quartz tube photolysis chamber. While the proxy calibration method was conducted in N_2 for this manuscript, it is possible to instead perform this method using air in the case that N_2 is incompatible with an instrument (unlike our CIMS). In an air-based proxy calibration, the $[\text{O}_3]$ produced by O_2 photolysis would need to be quantified (during dry conditions) and then subtracted from subsequent background subtracted NO_2 signals. but at the expense of greater calibration uncertainty. In conclusion, these photolytic calibration techniques offer a valuable alternative to the more conventional HONO calibration that is based on reacting hydrogen chloride vapor with sodium nitrite.

Deleted: generally

Deleted: 8

Deleted: 20

Deleted: 30

Deleted: to 36

440 *Data availability.* The data used in this manuscript is available upon request.

445 *Author contributions.* AJL and ECW designed the experiments. AJL carried them out and performed the data analysis. AJL prepared the manuscript with contributions from ECW.

Competing Interests. The authors declare that they have no conflict of interest.

Acknowledgements. We acknowledge financial support from Directorate for Geosciences of the National Science Foundation. This work was supported by NSF grant AGS-2002928. We are grateful to Phil Stevens (Indiana University) for characterizing the mercury lamp used for these calibrations.

450 References

Bertram, T., Kimmel, J., Crisp, T., Ryder, O., Yatavelli, R., Thornton, J., Cubison, M., Gonin, M., and Worsnop, D.: A field-deployable, chemical ionization time-of-flight mass spectrometer, *Atmospheric Measurement Techniques*, 4, 1471-1479, <https://doi.org/10.5194/amt-4-1471-2011>, 2011.

460 Bloss, W., Lee, J., Heard, D., Salmon, R. A., Bauguitte, S.-B., Roscoe, H., and Jones, A.: Observations of OH and HO₂ radicals in coastal Antarctica, *Atmospheric Chemistry and Physics*, 7, 4171-4185, <https://doi.org/10.5194/acp-7-4171-2007>, 2007.

Bottorff, B., Reidy, E., Mielke, L., Dusanter, S., and Stevens, P. S.: Development of a laser-photofragmentation laser-induced fluorescence instrument for the detection of nitrous acid and hydroxyl radicals in the atmosphere, *Atmospheric Measurement Techniques*, 14, 6039-6056, <https://doi.org/10.5194/amt-14-6039-2021>, 2021.

465 Bourgeois, I., Peischl, J., Neuman, J. A., Brown, S. S., Allen, H. M., Campuzano-Jost, P., Coggon, M. M., DiGangi, J. P., Diskin, G. S., Gilman, J. B., Gkatzelis, G. I., Guo, H., Halliday, H., Hanisco, T. F., Holmes, C. D., Huey, L. G., Jimenez, J. L., Lamplugh, A. D., Lee, Y. R., Lindaas, J., Moore, R. H., Nowak, J. B., Pagonis, D., Rickly, P. S., Robinson, M. A., Rollins, A. W., Selimovic, V., St. Clair, J. M., Tanner, D., Vasquez, K. T., Veres, P. R., Warneke, C., Wennberg, P. O., Washenfelder, R. A., Wiggins, E. B., Womack, C. C., Xu, L., Zarzana, K. J., and Ryerson, T. B.: Comparison of airborne measurements of NO, NO₂, HONO, NO_Y and CO during FIREX-AQ, <https://doi.org/10.5194/amt-2021-432>, in review, 2022.

470 Burkholder, J., Sander, S., Abbatt, J., Barker, J., Cappa, C., Crounse, J., Dibble, T., Huie, R., Kolb, C., and Kurylo, M.: Chemical kinetics and photochemical data for use in atmospheric studies, Evaluation No. 19, JPL Publication 19-10, Jet Propulsion Laboratory, Pasadena, 583-586, 2020.

475 Butkovskaya, N., Kukui, A., and Le Bras, G.: HNO₃ Forming Channel of the HO₂+ NO Reaction as a Function of Pressure and Temperature in the Ranges of 72– 600 Torr and 223– 323 K, *The Journal of Physical Chemistry A*, 111, 9047-9053, <https://doi.org/10.1021/jp074117m>, 2007.

Butkovskaya, N., Rayez, M.-T., Rayez, J.-C., Kukui, A., and Le Bras, G.: Water vapor effect on the HNO₃ yield in the HO₂+ NO reaction: experimental and theoretical evidence, *The Journal of Physical Chemistry A*, 113, 11327-11342, <https://doi.org/10.1021/jp811428p>, 2009.

480 Cheng, P., Cheng, Y., Lu, K., Su, H., Yang, Q., Zou, Y., Zhao, Y., Dong, H., Zeng, L., and Zhang, Y.: An online monitoring system for atmospheric nitrous acid (HONO) based on stripping coil and ion chromatography, *Journal of Environmental Sciences*, 25, 895-907, [https://doi.org/10.1016/s1001-0742\(12\)60251-4](https://doi.org/10.1016/s1001-0742(12)60251-4), 2013.

Crilley, L. R., Kramer, L. J., Ouyang, B., Duan, J., Zhang, W., Tong, S., Ge, M., Tang, K., Qin, M., Xie, P., Shaw, M. D., Lewis, A. C., Mehra, A., Bannan, T. J., Worrall, S. D., Priestley, M., Bacak, A., Coe, H., Allan, J., Percival, C. J., Popoola, O. A. M.,

485 Jones, R. L., and Bloss, W. J.: Intercomparison of nitrous acid (HONO) measurement techniques in a megacity (Beijing), *Atmospheric Measurement Techniques*, 12, 6449-6463, <https://doi.org/10.5194/amt-12-6449-2019>, 2019.

Dixneuf, S., Ruth, A. A., Häseler, R., Brauers, T., Rohrer, F., and Dorn, H.-P.: Detection of nitrous acid in the atmospheric simulation chamber SAPHIR using open-path incoherent broadband cavity-enhanced absorption spectroscopy and extractive long-path absorption photometry, *Atmospheric Measurement Techniques*, 15, 945-964, <https://doi.org/10.5194/amt-15-945-2022>, 2022.

490 Dusanter, S., Vimal, D., and Stevens, P.: Measuring tropospheric OH and HO₂ by laser-induced fluorescence at low pressure. A comparison of calibration techniques, *Atmospheric Chemistry and Physics*, 8, 321-340, <https://doi.org/10.5194/acp-8-321-2008>, 2008.

495 Dyson, J. E., Boustead, G. A., Fleming, L. T., Blitz, M., Stone, D., Arnold, S. R., Whalley, L. K., and Heard, D. E.: Production of HONO from NO₂ uptake on illuminated TiO₂ aerosol particles and following the illumination of mixed TiO₂ ammonium nitrate particles, *Atmospheric Chemistry and Physics*, 21, 5755-5775, <https://doi.org/10.5194/acp-21-5755-2021>, 2021.

500 Faloona, I. C., Tan, D., Lesher, R. L., Hazen, N. L., Frame, C. L., Simpas, J. B., Harder, H., Martinez, M., Di Carlo, P., and Ren, X.: A laser-induced fluorescence instrument for detecting tropospheric OH and HO₂: Characteristics and calibration, *Journal of Atmospheric Chemistry*, 47, 139-167, <https://doi.org/10.1023/B:JOCH.0000021036.53185.0e>, 2004.

505 Febo, A., Perrino, C., Gherardi, M., and Sparapani, R.: Evaluation of a high-purity and high-stability continuous generation system for nitrous acid, *Environmental science & technology*, 29, 2390-2395, <https://doi.org/10.1021/es00009a035>, 1995.

Gingerysty, N. J. and Osthoff, H. D.: A compact, high-purity source of HONO validated by Fourier transform infrared and thermal-dissociation cavity ring-down spectroscopy, *Atmospheric Measurement Techniques*, 13, 4159-4167, <https://doi.org/10.5194/amt-13-4159-2020>, 2020.

510 Gomez Alvarez, E., Amedro, D., Afif, C., Gligorovski, S., Schoemaecker, C., Fittschen, C., Doussin, J.-F., and Wortham, H.: Unexpectedly high indoor hydroxyl radical concentrations associated with nitrous acid, *Proceedings of the National Academy of Sciences*, 110, 13294-13299, <https://doi.org/10.1073/pnas.1308310110>, 2013.

515 Jaeglé, L., Shah, V., Thornton, J., Lopez-Hilfiker, F., Lee, B., McDuffie, E., Fibiger, D., Brown, S., Veres, P., and Sparks, T.: Nitrogen oxides emissions, chemistry, deposition, and export over the Northeast United States during the WINTER aircraft campaign, *Journal of Geophysical Research: Atmospheres*, 123, 12,368-312,393, <https://doi.org/10.1029/2018JD029133>, 2018.

Jiang, Y., Xue, L., Shen, H., Dong, C., Xiao, Z., and Wang, W.: Dominant Processes of HONO Derived from Multiple Field Observations in Contrasting Environments, *Environmental Science & Technology Letters*, 9, 258-264, <https://doi.org/10.1021/acs.estlett.2c00004>, 2022.

520 Jiang, Y., Xue, L., Gu, R., Jia, M., Zhang, Y., Wen, L., Zheng, P., Chen, T., Li, H., and Shan, Y.: Sources of nitrous acid (HONO) in the upper boundary layer and lower free troposphere of the North China Plain: insights from the Mount Tai Observatory, *Atmospheric Chemistry and Physics*, 20, 12115-12131, <https://doi.org/10.5194/acp-20-12115-2020>, 2020.

Kebabian, P. L., Wood, E. C., Herndon, S. C., and Freedman, A.: A practical alternative to chemiluminescence-based detection of nitrogen dioxide: Cavity attenuated phase shift spectroscopy, *Environmental science & technology*, 42, 6040-6045, <https://doi.org/10.1021/es703204j>, 2008.

525 Lanzendorf, E., Hanisco, T., Donahue, N., and Wennberg, P.: Comment on: "The measurement of tropospheric OH radicals by laser-induced fluorescence spectroscopy during the POPCORN Field Campaign" by Hofzumahaus et al. and "Intercomparison of tropospheric OH radical measurements by multiple folded long-path laser absorption and laser induced fluorescence" by Brauers et al, *Geophysical research letters*, 24, 3037-3038, <https://doi.org/10.1029/97GL02899>, 1997.

Lao, M., Crilley, L. R., Salehpoor, L., Furlani, T. C., Bourgeois, I., Neuman, J. A., Rollins, A. W., Veres, P. R., Washenfelder, R. A., Womack, C. C., Young, C. J., and VandenBoer, T. C.: A portable, robust, stable, and tunable calibration source for gas-phase nitrous acid (HONO), *Atmospheric Measurement Techniques*, 13, 5873-5890, <https://doi.org/10.5194/amt-13-5873-2020>, 2020.

530 Lee, B., Wood, E., Wormhoudt, J., Shorter, J., Herndon, S., Zahniser, M., and Munger, J.: Effective line strengths of trans-nitrous acid near 1275 cm⁻¹ and cis-nitrous acid at 1660 cm⁻¹, *Journal of Quantitative Spectroscopy and Radiative Transfer*, 113, 1905-1912, <https://doi.org/10.1016/j.jqsrt.2012.06.004>, 2012.

Lee, B. H., Lopez-Hilfiker, F. D., Mohr, C., Kurtén, T., Worsnop, D. R., and Thornton, J. A.: An iodide-adduct high-resolution time-of-flight chemical-ionization mass spectrometer: Application to atmospheric inorganic and organic compounds, *Environmental science & technology*, 48, 6309-6317, <https://doi.org/10.1021/es500362a>, 2014.

Li, X., Rohrer, F., Hofzumahaus, A., Brauers, T., Häseler, R., Bohn, B., Broch, S., Fuchs, H., Gomm, S., and Holland, F.:
535 Missing gas-phase source of HONO inferred from Zeppelin measurements in the troposphere, *Science*, 344, 292-296, <https://doi.org/10.1126/science.1248999>, 2014.

Lu, K., Fuchs, H., Hofzumahaus, A., Tan, Z., Wang, H., Zhang, L., Schmitt, S. H., Rohrer, F., Bohn, B., and Broch, S.: Fast photochemistry in wintertime haze: consequences for pollution mitigation strategies, *Environmental science & technology*, 53, 10676-10684, <https://doi.org/10.1021/acs.est.9b02422>, 2019.

540 Novak, G. A., Vermeuel, M. P., and Bertram, T. H.: Simultaneous detection of ozone and nitrogen dioxide by oxygen anion chemical ionization mass spectrometry: a fast-time-response sensor suitable for eddy covariance measurements, *Atmospheric Measurement Techniques*, 13, 1887-1907, <https://doi.org/10.5194/amt-13-1887-2020>, 2020.

Peng, Q., Palm, B. B., Melander, K. E., Lee, B. H., Hall, S. R., Ullmann, K., Campos, T., Weinheimer, A. J., Apel, E. C., and Hornbrook, R. S.: HONO emissions from western US wildfires provide dominant radical source in fresh wildfire smoke,
545 Environmental science & technology, 54, 5954-5963, <https://doi.org/10.1021/acs.est.0c00126>, 2020.

Pinto, J. P., Dibb, J., Lee, B. H., Rappenglück, B., Wood, E. C., Levy, M., Zhang, R. Y., Lefer, B., Ren, X. R., Stutz, J., Tsai, C., Ackermann, L., Golovko, J., Herndon, S. C., Oakes, M., Meng, Q. Y., Munger, J. W., Zahniser, M., and Zheng, J.: Intercomparison of field measurements of nitrous acid (HONO) during the SHARP campaign, *Journal of Geophysical Research: Atmospheres*, 119, 5583-5601, <https://doi.org/10.1002/2013jd020287>, 2014.

550 Ren, X., Van Duin, D., Cazorla, M., Chen, S., Mao, J., Zhang, L., Brune, W. H., Flynn, J. H., Grossberg, N., and Lefer, B. L.: Atmospheric oxidation chemistry and ozone production: Results from SHARP 2009 in Houston, Texas, *Journal of Geophysical Research: Atmospheres*, 118, 5770-5780, <https://doi.org/10.1002/jgrd.50342>, 2013.

Schultz, M., Heitlinger, M., Mihelcic, D., and Volz-Thomas, A.: Calibration source for peroxy radicals with built-in actinometry using H₂O and O₂ photolysis at 185 nm, *Journal of Geophysical Research: Atmospheres*, 100, 18811-18816, <https://doi.org/10.1029/95JD01642>, 1995.

Slater, E. J., Whalley, L. K., Woodward-Massey, R., Ye, C., Lee, J. D., Squires, F., Hopkins, J. R., Dunmore, R. E., Shaw, M., and Hamilton, J. F.: Elevated levels of OH observed in haze events during wintertime in central Beijing, *Atmospheric Chemistry and Physics*, 20, 14847-14871, <https://doi.org/10.5194/acp-20-14847-2020>, 2020.

560 Stevens, P., Mather, J., and Brune, W.: Measurement of tropospheric OH and HO₂ by laser-induced fluorescence at low pressure, *Journal of Geophysical Research: Atmospheres*, 99, 3543-3557, <https://doi.org/10.1029/93JD03342>, 1994.

Stutz, J., Oh, H.-J., Whitlow, S. I., Anderson, C., Dibb, J. E., Flynn, J. H., Rappenglück, B., and Lefer, B.: Simultaneous DOAS and mist-chamber IC measurements of HONO in Houston, TX, *Atmospheric Environment*, 44, 4090-4098, <https://doi.org/10.1016/j.atmosenv.2009.02.003>, 2010.

Tuite, K., Thomas, J. L., Veres, P. R., Roberts, J. M., Stevens, P. S., Griffith, S. M., Dusanter, S., Flynn, J. H., Ahmed, S., and Emmons, L.: Quantifying nitrous acid formation mechanisms using measured vertical profiles during the CalNex 2010 campaign and 1D column modeling, *Journal of Geophysical Research: Atmospheres*, 126, e2021JD034689, <https://doi.org/10.1029/2021JD034689>, 2021.

Veres, P. R., Neuman, J. A., Bertram, T. H., Assaf, E., Wolfe, G. M., Williamson, C. J., Weinzierl, B., Tilmes, S., Thompson, C. R., and Thames, A. B.: Global airborne sampling reveals a previously unobserved dimethyl sulfide oxidation mechanism in the

570 marine atmosphere, *Proceedings of the National Academy of Sciences*, 117, 4505-4510,
<https://doi.org/10.1073/pnas.1919344117>, 2020.

Veres, P. R., Roberts, J. M., Wild, R. J., Edwards, P. M., Brown, S. S., Bates, T. S., Quinn, P. K., Johnson, J. E., Zamora, R. J., and de Gouw, J.: Peroxynitric acid (HO_2NO_2) measurements during the UBWOS 2013 and 2014 studies using iodide ion chemical ionization mass spectrometry, *Atmospheric Chemistry and Physics*, 15, 8101-8114, <https://doi.org/10.5194/acp-15-8101-2015>, 2015.

Villena, G. and Kleffmann, J.: A source for the continuous generation of pure and quantifiable HONO mixtures, *Atmospheric Measurement Techniques*, 15, 627-637, <https://doi.org/10.5194/amt-15-627-2022>, 2022.

Villena, G., Kleffmann, J., Kurtenbach, R., Wiesen, P., Lissi, E., Rubio, M. A., Croxatto, G., and Rappenglück, B.: Vertical gradients of HONO, NOx and O₃ in Santiago de Chile, *Atmospheric Environment*, 45, 3867-3873, <https://doi.org/10.1016/j.atmosenv.2011.01.073>, 2011.

580 Wang, C., Bottorff, B., Reidy, E., Rosales, C. M. F., Collins, D. B., Novoselac, A., Farmer, D. K., Vance, M. E., Stevens, P. S., and Abbatt, J. P.: Cooking, bleach cleaning, and air conditioning strongly impact levels of HONO in a house, *Environmental Science & Technology*, 54, 13488-13497, <https://doi.org/10.1021/acs.est.0c05356>, 2020.

Whalley, L. K., Stone, D., Dummore, R., Hamilton, J., Hopkins, J. R., Lee, J. D., Lewis, A. C., Williams, P., Kleffmann, J., and 585 Laufs, S.: Understanding in situ ozone production in the summertime through radical observations and modelling studies during the Clean air for London project (ClearfLo), *Atmospheric Chemistry and Physics*, 18, 2547-2571, <https://doi.org/10.5194/acp-18-2547-2018>, 2018.

Wong, K., Tsai, C., Lefer, B., Haman, C., Grossberg, N., Brune, W., Ren, X., Luke, W., and Stutz, J.: Daytime HONO vertical gradients during SHARP 2009 in Houston, TX, *Atmospheric Chemistry and Physics*, 12, 635-652, <https://doi.org/10.5194/acp-12-635-2012>, 2012.

590 Ye, C., Gao, H., Zhang, N., and Zhou, X.: Photolysis of Nitric Acid and Nitrate on Natural and Artificial Surfaces, *Environ Sci Technol*, 50, 3530-3536, <https://doi.org/10.1021/acs.est.5b05032>, 2016.

Ye, C., Zhang, N., Gao, H., and Zhou, X.: Photolysis of Particulate Nitrate as a Source of HONO and NOx, *Environ Sci Technol*, 51, 6849-6856, <https://doi.org/10.1021/acs.est.7b00387>, 2017.

595 York, D., Evensen, N. M., Martinez, M. L., and De Basabe Delgado, J.: Unified equations for the slope, intercept, and standard errors of the best straight line, *American Journal of Physics*, 72, 367-375, <https://doi.org/10.1119/1.1632486>, 2004.

Young, C. J., Washenfelder, R. A., Roberts, J. M., Mielke, L. H., Osthoff, H. D., Tsai, C., Pikelnaya, O., Stutz, J., Veres, P. R., Cochran, A. K., VandenBoer, T. C., Flynn, J., Grossberg, N., Haman, C. L., Lefer, B., Stark, H., Graus, M., de Gouw, J., Gilman, J. B., Kuster, W. C., and Brown, S. S.: Vertically resolved measurements of nighttime radical reservoirs in Los Angeles 600 and their contribution to the urban radical budget, *Environ Sci Technol*, 46, 10965-10973, <https://doi.org/10.1021/es302206a>, 2012.